Institute of Research and Publication Indonesia (IRPI)
Public Research Journal of Engineering, Data Technology and Computer Science
Journal Homepage: https://journal.irpi.or.id/index.php/predatecs
Vol. 3 Iss. 1 July 2025, pp: 10-21
ISSN(P): 3024-921X | ISSN(E): 3024-8043

Deep Learning for Pneumonia Detection in Chest X-Rays using Different Algorithms and Transfer Learning Architectures

Danur Lestari[1*], Anggi Mulya[2], Aghnia Tatamara[3], Ryando Rama Haiban[4], Habibah Dian Khalifah[5]

[1,2]Department of Information Systems, Faculty of Science and Technology,
Universitas Islam Negeri Sultan Syarif Kasim Riau, Indonesia
[3]Dapartment of Business Management, Faculty of Economics and Administrative Sciences,
Dokuz Eylul University, Turkey
[4]Dapartment of Management Information System, Faculty of Economics and Administrative Sciences,
Dokuz Eylul University, Turkey
[5]Dapartment of Ushuluddin, Faculty of Sharia, Yarmouk University, Jordan

E-Mail: [1]12150321355@students.uin-suska.ac.id, [2]12150312142@students.uin-suska.ac.id,
[3]aghniatatamara4@gmail.com, [4]ryandohaibaan@gmail.com, [5]habibahdian7@gmail.com

Received Jul 17th 2024; Revised Mar 26th 2025; Accepted Apr 14th 2025; Available Online Jul 05th 2025, Published Jul 31th 2025
Corresponding Author: Danur Lestari

Abstract

Pneumonia is one of the lung conditions brought on by bacterial infections. An accurate diagnosis is necessary for successful treatment. A radiologist can typically diagnose the condition based on images from a chest X-ray. The diagnosis may be arbitrary for a variety of reasons, such as the indistinctness of certain diseases on chest X-ray pictures or the possibility of the illness being mistaken for another. Consequently, clinicians require guidance from computer-aided diagnosis tools. We diagnosed pneumonia using two algorithms Convolutional Neural Network (CNN) and Generative Adversarial Network (GAN), as well as two architectures ResNet50V2 and InceptionV3. The test results show that the ResNet50V2 architecture is superior to the InceptionV3 architecture on the CNN algorithm with an accuracy of 94% versus 93%. In addition, the test results on the GANs algorithm show that the ResNet50V2 architecture is superior to the InceptionV3 architecture with an accuracy of 96%, while the InceptionV3 architecture achieves an accuracy of 92%.

Keyword: Convolutional Neural Network, Generative Adversarial Network, InceptionV3, Pneumonia, ResNet50V2

1. INTRODUCTION

Early detection is a critical factor in preventing pneumonia, a disease caused by bacteria, viruses, fungi, or other microorganisms, which remains a significant global health challenge. Worldwide, pneumonia is responsible for more than 740,000 deaths among children under the age of five and claims over 41,000 adult lives annually in the United States alone [1], [2], [3]. Despite advancements in healthcare, the high mortality rate underscores the need for timely and accurate diagnosis to facilitate effective treatment and improve patient outcomes.

Chest X-ray imaging is a cornerstone in the diagnosis of pneumonia, as it provides a clear visual representation of the lungs, allowing medical professionals to identify infection-related abnormalities. However, the manual interpretation of X-rays by radiologists is inherently challenging due to the complexity of the images, the variability in disease presentation, and the reliance on the radiologist's expertise and experience [4], [5], [6], [7]. This process can be time-intensive, prone to human error, and often inconsistent, especially in regions facing a shortage of skilled radiologists or an overwhelming number of cases. The urgency of this research is driven by the rising prevalence of pneumonia and the associated strain on healthcare systems, which hinder the efficiency and accuracy of manual diagnosis. An automated diagnostic solution leveraging advanced image analysis techniques has the potential to address these challenges, reducing diagnostic delays and improving reliability. By streamlining the detection process, such technology can significantly enhance the quality of patient care and contribute to reducing pneumonia-related mortality. Therefore, this study aims to develop a robust, effective, and accessible automated diagnostic tool to meet this pressing need.

In this case, deep learning techniques are needed to obtain accurate identification [8]. It has been demonstrated that Convolutional Neural Network (CNN) and Generative Adversarial Network (GAN) are also

very capable of automating the categorization of pneumonia from chest X-ray images [9], [10]. Finding pneumonia is one of the many medical imaging tasks that CNNs have proved successful at [11]. Additionally, because CNNs can recognize hierarchical features in images, they are frequently utilized in medical image analysis. CNNs usually consist of multiple layers of pooling and convolution before the layers are fully connected. This allows the network to extract shapes, textures, and patterns from images, which can be used to classify images [12], [13].

A generator and a discriminator are the two neural networks that make up a GAN. Once the discriminator has rendered a judgment, the generator creates a synthetic image that closely resembles the original. GANs have proven effective in both image production and image-to-image translation. They can generate synthetic X-ray images that are similar to actual images for pneumonia categorization, which can be utilized to train Convolutional Neural Networks (CNNs) [14], [15], [16]. One significant advantage of GANs is their ability to produce high-quality synthetic images that can augment training datasets, improving the robustness of models and enabling better generalization to unseen data.

In this study, the ResNet and InceptionV3 transfer learning architectures were used along with the Mendeley dataset. CNNs are particularly advantageous for image analysis due to their ability to automatically learn hierarchical features from images, enabling them to capture complex patterns essential for accurate diagnosis. Previous studies using different transfer learning architectures, such as Ayan [17], who utilized Xception and VGG16 architectures to diagnose pneumonia, demonstrated that Xception was particularly effective in detecting pneumonia cases. Additionally, Rajpurkar [18] identified pneumonia through the ChexNet model neural network, a variant of the 121-layer DenseNet, showcasing the effectiveness of CNNs in medical image classification.

The combination of CNN and GAN has shown improved performance in pneumonia classification tasks. By utilizing the advantages of both models, researchers can create a more accurate and robust classification system. While GAN can produce synthetic images that resemble the actual images, CNN can extract features from X-ray images. This can help the model become more generalized and less prone to overfitting [19], [20].

The growing workload of radiologists and the inconsistent outcomes of human diagnosis processes highlight the pressing need for an automated system that can diagnose pneumonia quickly and accurately. This paper proposes a novel method to improve the efficacy and precision of pneumonia recognition by combining the usage of GAN integration with the ResNet50V2 and InceptionV3 architectures. In contrast to previous studies that used architectures such as Xception, VGG16, and DenseNet, this study focuses on evaluating the effectiveness of the combination of architectures and GAN integration to create a more robust and capable model. It is anticipated that the findings of this study will contribute to the development of a pneumonia categorization system that is more precise and useful. In the end, this will result in better treatment outcomes and healthcare services as a whole.

2. MATERIAL AND METHOD

2.1. Methodology

This research focuses on X-ray classification of pneumonia diseases using the Kaggle dataset. To conduct this research, Google Collabs was used as the chosen tool to compare two algorithms: CNN and GAN. Thus, the researcher conducted the research stages as shown in Figure 1.

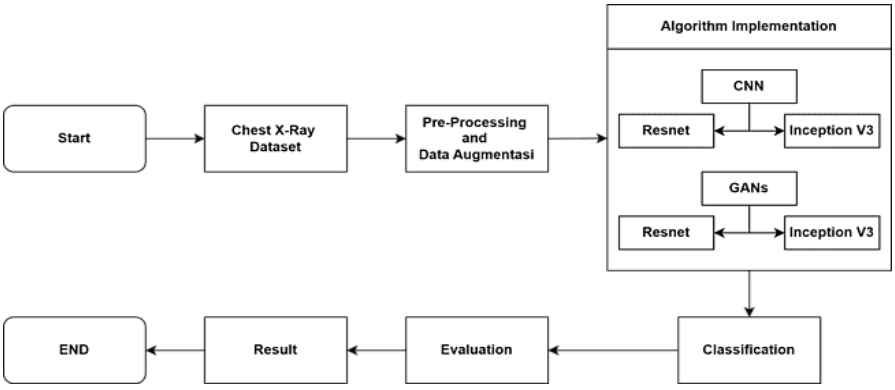

Figure 1. Research Methodology

The workflow in this research on the classification of pneumonia X-rays begins with data collection from the Kaggle dataset, which contains X-ray images of lungs labeled as pneumonia or non-pneumonia. Once the data is collected, the next step is preprocessing, where the data is processed to enhance image quality. This process includes resizing the images, normalizing pixel values, and augmenting the data to increase dataset

diversity. Subsequently, two different models are applied: CNN, using architectures such as ResNet and InceptionV3 for image classification, and GAN, which generate synthetic X-ray images that resemble actual images to enrich the dataset. After training the models with the processed and enhanced dataset, model evaluation is conducted using metrics such as accuracy, precision, recall, and F1-score to assess their performance in classifying X-ray images. Finally, the results from the model evaluation are analyzed to draw conclusions about the effectiveness of each algorithm in pneumonia classification.

2.2. Dataset

Mendeley's Labeled Optical Coherence Tomography (OCT) and the Chest X-Ray Image dataset, which comprises 5,860 X-Ray images in JPEG format, were used in this investigation. Both datasets were donated by Kermany [21]. A retrospective cohort of pediatric patients from Guangzhou Women and Children's Medical Center, Guangzhou, was used to choose chest X-ray images (anterior-posterior). Three primary directories comprise the dataset: the train folder, test folder, and val folder. Every directory has two subdirectories: one with X-ray pictures of pneumonia and the other with X-ray pictures of healthy lungs. Figure 2 shows a normal chest x-ray with clear lungs and no abnormal opacities. Bacterial pneumonia (center) usually shows isolated lobar consolidation, as in this case in the right upper lobe (white arrow), while viral pneumonia displays a more diffused "interstitial" pattern in both lungs. Table 1 shows the amount of image data collected for the training, validation, and testing phases of the suggested model.

Figure 2. Sample Data from The Dataset

Table 1. Number of Image Datasets

Class	Train	Val	Test
Pneumonia	3420	855	855
Normal	1268	317	317
Total	4688	1172	1172

2.3. Convolutional Neural Networks (CNN)

Artificial intelligence (AI)-based solutions have been explored by numerous academics and studies in recent years to address a variety of medical issues. Artificial Neural Networks (ANNs) have proven effective in treating a wide range of ailments, including breast cancer, brain tumors, and disease classification using X-ray images [22]. Figure 3 illustrates CNN's fundamental idea.

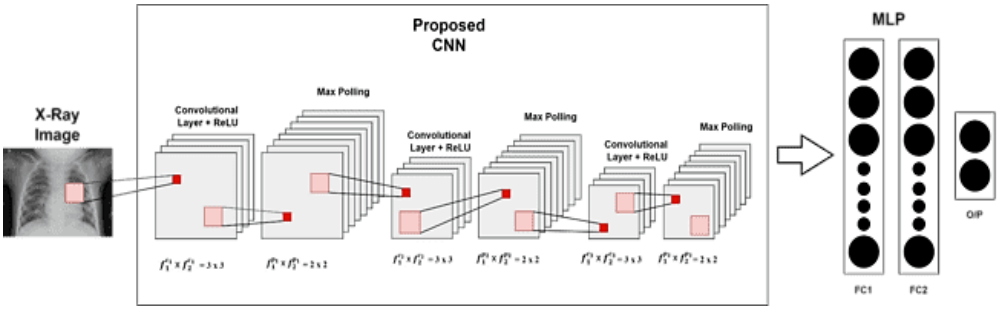

Figure 3. A simple idea of a CNN

According to Convolutional Neural Networks, the input type is an image. They also believe that contemporary deep learning models in computer vision are better suited to CNNs because they can detect low-level aspects in images, such as edges, and use filters to gather temporal and spatial dependencies [23]. CNNs further minimize calculation time because each layer consists of filters or kernels and the weight sharing algorithm is lower-parameterized. Because of the spatial extent of the representation created by the preceding kernel following convolution, the pooling layer aids in the extraction of dominating features that remain constant in position and rotation. Placing this layer between two equal convolution layers, the most popular layer is the maximum pooling layer, which "separates the input into boxes of a certain size, and outputs the

maximum value from each box". Furthermore, the average of every box is determined using the y average pooling layer. When it comes to lowering the dimensionality and needed computing effort, these two methods are quite successful. In light of its successes and advancements in the identification of pneumonia, CNN performs significantly better on larger data sets, but its effectiveness on smaller data sets is dependent on its proper application [24].

2.4. Generative Adversarial Network (GANs)

The Generative Adversarial Network is a very new and powerful tool that can produce images using a min-max approach in an unsupervised manner [25]. A few of the image generation and manipulation tasks in which GANs have proven to be very beneficial are text-to-image synthesis [26], super-resolution (producing high-resolution images from low-resolution images) [27], image-to-image translation (e.g., converting sketches into images) [28], and image blending (e.g., combining sketches into images) [29]. GAN uses two competing networks (x), G(z) and D. The generator G(z) tricks the discriminator D(z) by producing photorealistic images. Stated differently, the discriminator's job is to maximize the function V(D,G)'s cost, while the generator's is to reduce it [30], [31]. The following Figure 4 shows the concept.

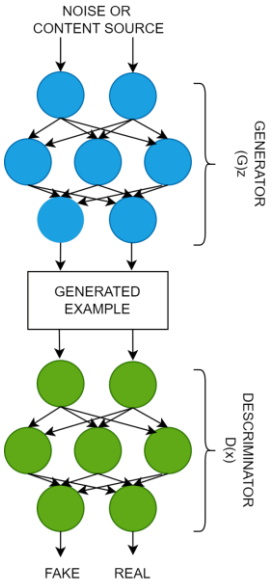

Figure 4. A simple idea of GANs

2.5. ResNet50V2

The computer vision and deep learning communities hold ResNet50V2 in high regard because it offers superior performance over AlexNet even when training extremely complex neural networks with hundreds or thousands of layers. The usage of brief connections or jumps, which aids the network in overcoming the issue of vanishing gradients and accuracy loss, is one of ResNet50V2's primary advantages [32]. Figure 5 shows the design of ResNet50V2.

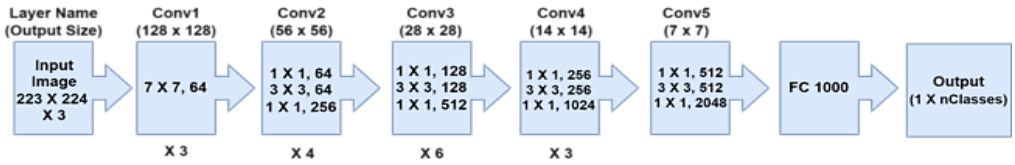

Figure 5. ResNet50V2 Architecture

In addition, it reduces instruction errors and speeds up network unification. ResNet50V2 terdiri dari lima tahap yang masing-masing berisi tiga lapisan konvolusi dan blok konvolusi dan identitas. Ada juga lebih dari 23 juta parameter yang dapat dilatih. A shortcut identity mapping is used to reduce errors and computation time. This mapping explicitly allows the layers to interact with the residual mapping and shows it as H(x). In addition, non-linear layers can interact with another mapping F(x): =H(x)-x. As a result, the initial mapping becomes H(x) :=F(x) + xH(x) :=F(x) + x [31].

2.6. InceptionV3

By computing 1 x 1 and 3 x 3 convolutions, the InceptionV3 Model increases the depth and width of the deep learning network. Overall, the model works well by retrieving the results from all the kernel types present in the image [32]. By using convolution factorization to reduce the number of connections and parameters, InceptionV3 does not reduce network efficiency. It has a depth of 42 layers and the computational cost is only about 2.5 higher than GoogleNet. Incremental Classifier is used as a regularizer that reduces the network size effectively in InceptionV3. Label alignment is used to keep the largest logistics from becoming much larger than the others. InceptionV3 becomes more efficient and cheaper thanks to these features. Figure 6 shows the design of InceptionV3.

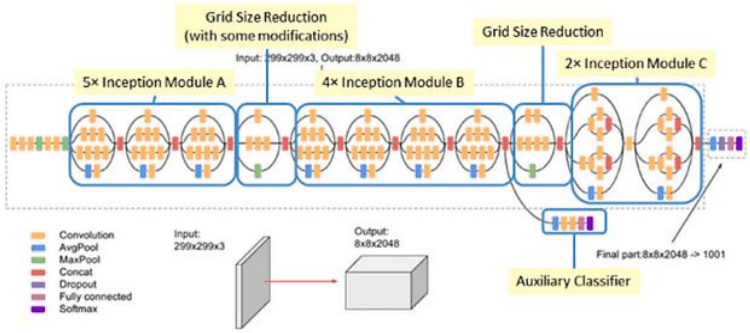

Figure 6. InceptionV3 Architecture

2.7. Confusion Metrics

Performance metrics such as accuracy, precision, recall, and F1 score are used to evaluate the proposed architecture. The formulas for these metrics are given the equation 1 – 4.

$$\text{Precision} = \frac{TP}{TP + FP} \times 100\% \quad (1)$$

$$\text{Recall} = \frac{TP}{TP + FN} \times 100\% \quad (2)$$

$$\text{Accuracy} = \frac{TP + TN}{TP + FN + TN + FP} \times 100\% \quad (3)$$

$$\text{F1} = \frac{precision \times recall}{precision + recall} \times 100\% \quad (4)$$

TP, TN, FN, and FP represent true positive, negative positive, false negative, and false positive in equations (1) to (4), respectively.

3. RESULTS AND DISCUSSION

3.1. Preprocessing and Augmentasi Data

From the dataset previously described, data preprocessing is carried out by dividing the data 80% for training data and 20% for testing data from the division obtained training data as many as 4,688 images and testing data as many as 1,172 images, then the data is made into different directories. After the data is preprocessed then the data is augmented with random rotation up to 45 degrees, rescale image pixel value 1/255, shear angle value of 15%, random zoom of 15% and random flip vertically and horizontally. The results of the augmentation that has been done can be seen in Figure 7.

Figure 7. Data Augmentation

3.2. CNN ResNet50V2

The ResNet50V2 architecture was pre-trained on the ImageNet dataset as the basis for image classification. First, the ResNet50V2 base model was imported without the top classification layer (include_top=False) and with pre-trained weights (weights='imagenet'), as well as input images of size 224 x

224 x 3. All layers in this base model were then set as non-trainable to preserve the pre-trained weights and prevent changes during training. Next, the model was extended by adding custom classification layers.The first layer is GlobalAveragePooling2D, which converts the average value of a two-dimensional feature map into a one-dimensional vector. The next layer is a fully connected layer with 512 neurons and a ReLU activation function to learn complex data patterns. During training, 20% of the neurons were randomly deactivated. A dropout layer with a rate of 0.2 was added to avoid overfitting. Finally, binary classification was performed using an output layer with two neurons and a sigmoid activation function. After that, the following parameters were added: epoch size of 30, batch size of 128, applied learning rate of 0.001 and the optimizer used was Nadam. Figure 8 is the accuracy and loss graph of CNN ResNet50V2.

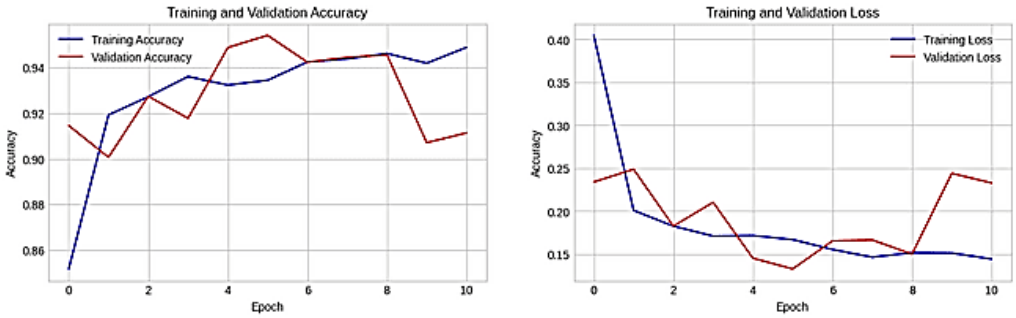

Figure 8. Accuracy and Loss Graph of CNN ResNet50V2

Figure 8 shows the model training results with accuracy and loss metrics for the training and validation data. In the accuracy graph, it can be seen that the accuracy increases rapidly in the first few epochs and reaches a stable high value around the 3rd epoch, with the validation accuracy fluctuating slightly more but remaining in a good range. In the loss graph, there is a significant decrease in the early epochs and the loss value tends to stabilize low after the 3rd epoch, although there are some fluctuations especially in the validation data. Overall, the model performs well with high accuracy and low loss, although there are some fluctuations in the validation data that need to be considered to ensure there is no sign of overfitting.

3.3. CNN InceptionV3

The InceptionV3 architecture was pre-trained on the ImageNet dataset as the basis for image classification. First, the InceptionV3 base model was imported without the top classification layer (include_top=False) and with pre-trained weights (weights='imagenet'), as well as input images of size 224 x 224 x 3. All layers in this base model were then set as non-trainable to preserve the pre-trained weights and prevent changes during training. Afterwards, more layers of custom classification were added to the model. The initial layer is in charge of ascertaining the input image's dimensions. Next, features are extracted from the image using the InceptionV3 core model. The two-dimensional feature map is reduced in size by the Global Average Pooling 2D layer to a one-dimensional vector with uniformly distributed values. Subsequently, a fully linked layer with 512 neurons and ReLU activation function is used to understand complicated data patterns. During training, half of the neurons are randomly deactivated. To avoid overfitting, a dropout layer with a rate of 0.2 is introduced. Lastly, for binary classification, an output layer comprising two neurons and a sigmoid activation function are employed. Next, the Nadam optimizer, learning rate of 0.001, batch size of 128 and epoch size of 30 were introduced. Figure 9 displays the InceptionV3 CNN's accuracy and loss graphs.

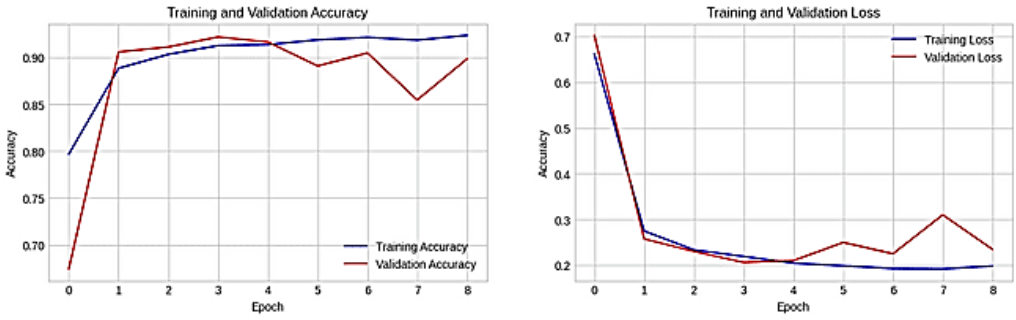

Figure 9. Accuracy and Loss Graph of InceptionV3 CNN

The accuracy and loss metrics for the training and validation data are displayed together with the model training outcomes in Figure 9. The accuracy graph shows that the validation accuracy fluctuates slightly more

but stays within a good range, while the accuracy grows quickly in the early epochs and reaches a steady high value around the second epoch. On the loss graph, there is a significant decrease in the initial epoch, with the loss value decreasing drastically until the 2nd epoch and then stabilizing low, although there are some small fluctuations in the validation data. Overall, the model performed well with high accuracy and low loss, although the fluctuations in the validation data show that the model needs to be watched to prevent overfitting.

3.4. GANs ResNet50V2

The ResNet50V2 architecture was pre-trained on the ImageNet dataset as the basis for image classification. First, the ResNet50V2 base model was imported without the top classification layer (include_top=False) with input images of size 224 x 224 x 3. The layers in this base model were frozen (trainable=False) to preserve the trained weights and prevent changes during training. Next, the model was extended by adding custom classification layers. Values of the two-dimensional feature map are averaged into a one-dimensional vector by GlobalAveragePooling2D in the first layer. Subsequently, complicated data patterns are learned using a fully linked layer that has 128 neurons and a ReLU activation function. Fifty percent of the neurons are silenced at random during training. A dropout layer with a rate of 0.5 is added to avoid overfitting. Lastly, an output layer with two neurons and a sigmoid activation function is employed for binary classification. Furthermore, the following parameters were added: epoch size 30, batch size 128, learning rate 0.001, and the AdamW optimizer was used. The accuracy and loss graphs of the ResNet50V2 GAN are shown in Figure 10.

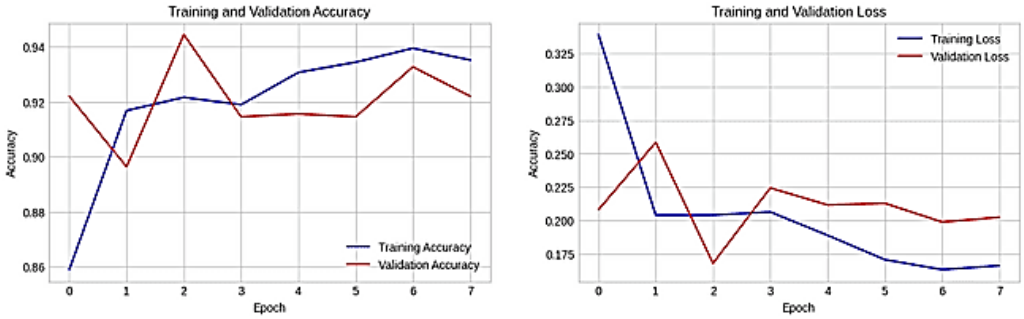

Figure 10. Accuracy and loss graphics of ResNet50V2 GANs

Figure 10 shows the changes in accuracy and loss during the training and validation of the model in 7 epochs. In the accuracy graph, it can be seen that the training accuracy (blue line) generally increases and stabilizes around 0.92 to 0.94 after the 2nd epoch. The validation accuracy (red line) shows larger fluctuations but tends to follow the same pattern as the training accuracy, reaching the highest value around 0.94 at the 2nd epoch. In the loss graph, the training loss (blue line) decreases sharply in the first epoch and stabilizes at a lower value after that. The validation loss (red line) also shows a significant decrease at the beginning, but larger fluctuations occur thereafter. Overall, the model shows good learning ability with high accuracy and low loss, although there are some fluctuations in the validation metrics that could indicate variations in performance on data that has not been seen before.

3.5. GANs InceptionV3

This InceptionV3 architecture utilizes two different architectures which are generator and classifier based. The generator aims to create a new image from random vectors by converting it into a 3D tensor through the Dense and Reshape layers, followed by the Conv2DTranspose layer to enlarge the image to the desired size with ReLU activation and tanh activation at the output layer. In contrast, the InceptionV3-based classifier extracts features from the input image using an architecture that has been trained on the ImageNet dataset. The Flatten layer is added to the feature map to turn it into a one-dimensional vector after the InceptionV3 layer has been frozen to maintain the trained weights. To learn complicated patterns and avoid overfitting, a thick layer with ReLU and Dropout activation is employed prior to the output layer with sigmoid activation for binary classification. Furthermore, the following parameters were added: epoch size 30, batch size 128, applied learning rate of 0.001, and the optimizer used was AdamW. The accuracy and loss graphs of the InceptionV3 JST are shown in Figure 11.

Figure 11 displays the variations in accuracy and loss over the model's 25 epochs of training and validation. The training accuracy (blue line) in the accuracy graph rises dramatically in the first few epochs before stabilizing at 0.9 after the fifth epoch. Though there are some minor oscillations, the validation accuracy (red line) likewise stabilizes at 0.9 and exhibits a similar pattern to the training accuracy. The training loss (blue line) and validation loss (red line) on the loss graph exhibit a steep decline in the first few epochs before nearly leveling out at a very low value. This demonstrates how the model effectively minimizes prediction

error right from the start of training and keeps up that performance throughout the remaining epochs. With both training and validation data, the model has a significant capacity for learning together with minimal loss and excellent accuracy.

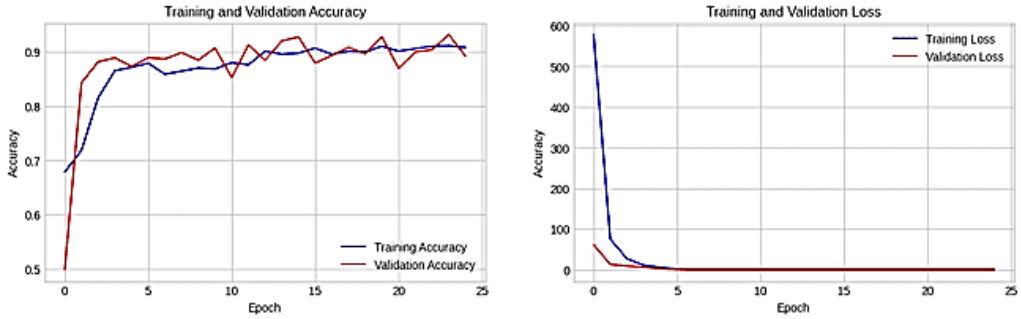

Figure 11. Accuracy and loss graphics of InceptionV3 GANs

These experimental results could be influenced by the quality of the dataset, data augmentation techniques, and InceptionV3's architecture which is effective in extracting hierarchical features. The stability of accuracy and low loss indicates the model is able to learn patterns well, but further analysis is needed to ascertain whether these results are influenced by key attributes such as the training or preprocessing parameters used.

3.6. Results

3.6.1. Confusion Matrics

Figure 12 shows that the ResNet50V2 CNN has a good performance in pneumonia detection. Out of 885 true normal cases, this model correctly classified 66 cases and misclassified 251 cases as pneumonia. Of the 855 true pneumonia cases, 181 were misclassified as normal, and 674 were correctly predicted as pneumonia. This model has the lowest error rate in classifying normal cases as pneumonia and is more accurate in correctly detecting pneumonia cases.

In Figure 13, the InceptionV3 CNN performs quite well but slightly lower than the ResNet50V2 CNN. Out of 885 true normal cases, CNN InceptionV3 correctly classified 88 cases and misclassified 229 cases as pneumonia. Of the 855 true pneumonia cases, 236 were misclassified as normal, and 619 were correctly predicted as pneumonia. Although there is an improvement in correctly detecting pneumonia cases compared to the ResNet50V2 CNN, there is still a fairly high error rate in classifying normal cases as pneumonia.

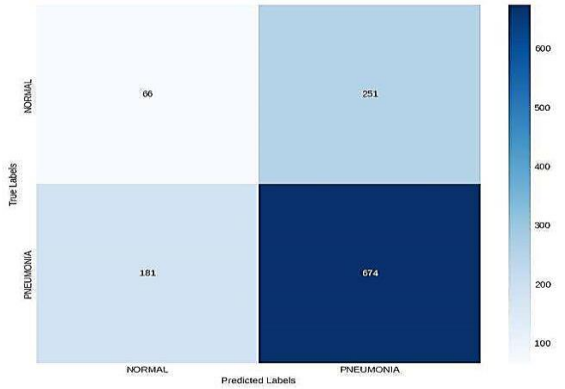

Figure 12. Confusion Metrics CNN ResNet50V2

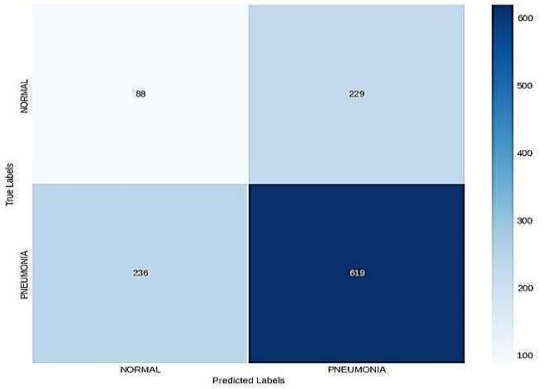

Figure 13. Confusion Metrics CNN InceptionV3

Figure 14 shows the performance of GANs ResNet50V2 which is between CNN ResNet and CNN Inception. Out of 885 true normal cases, ResNet50V2 GANs correctly classified 84 cases and misclassified 233 cases as pneumonia. Of the 855 true pneumonia cases, 233 were misclassified as normal, and 622 were correctly predicted as pneumonia. These ResNet50V2 GANs performed better than InceptionV3 GANs but slightly lower than InceptionV3 CNNs.

In Figure 15 GANsInceptionV3 has the lowest performance in pneumonia detection among all. Out of 885 true normal cases, GANsInceptionV3 correctly classified 103 cases and misclassified 214 cases as pneumonia. Of the 855 true pneumonia cases, 267 were misclassified as normal, and 588 were correctly predicted as pneumonia. GANsInceptionV3 had a high error rate in classifying normal cases as pneumonia and also had significant errors in classifying pneumonia cases as normal.

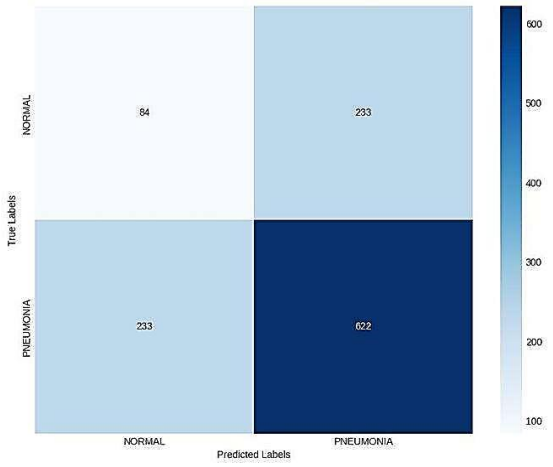

Figure 14. Confusion Metrics GANs ResNet50V2

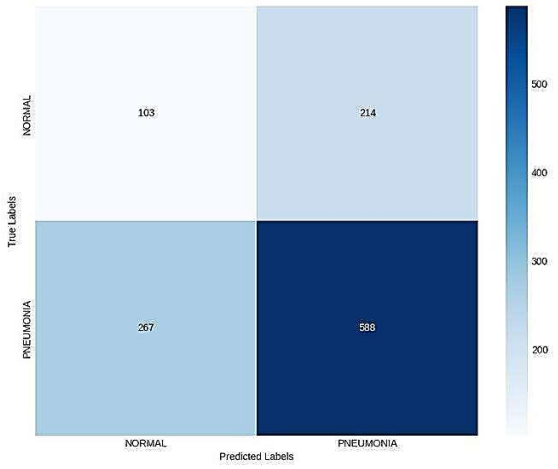

Figure 15. Confusion Metrics GANsInceptionV3

3.6.2. Accuracy Result

Table 2 shows a comparison of the accuracy results where the CNN ResNet50V2 model achieved an accuracy of 94%, while the CNN InceptionV3 model achieved an accuracy of 93%. The use of GANs improved accuracy in several models, with GANs ResNet50V2 achieving the highest accuracy of 96%, while GANs InceptionV3 showed a decrease in accuracy to 92%.

Table 2. Comparison of accuracy results

Algorithms	ResNet50V2	InceptionV3
CNN	94%	93%
GANs	96%	92%

3.6.3. Test Result

Figure 16 shows the test results of the ResNet50V2 CNN model on chest X-ray images to detect pneumonia. The model gives a probability of 77.20% for pneumonia, while the normal probability is 10.81%. This shows a fairly good performance in identifying pneumonia, although there is potential for improvement in the prediction of normal cases. Figure 17 displays the test results of the InceptionV3 CNN model on a chest X-ray image. The model produced a pneumonia probability of 85.07% and a normal probability of 57.31%. These results show that the model has a higher confidence level in detecting pneumonia, but there is a high possibility for errors in distinguishing between normal and pneumonia conditions.

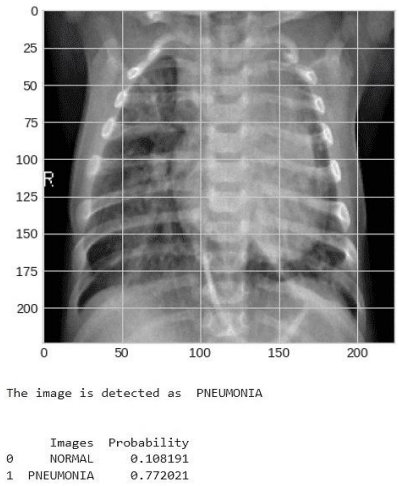

Figure 16. CNN ResNet50V2 test results

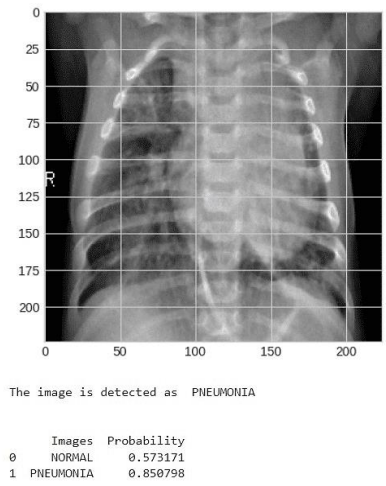

Figure 17. CNN InceptionV3 test results

Figure 18 Visualizes the test results of the ResNet50V2 GANs model. This model gives a probability of 75.85% for pneumonia and 11.13% for normal conditions. Although the results are similar to the ResNet50V2 CNN model, the use of GANs helps generate additional data that supports the model training. Figure 19 illustrates the test results of the InceptionV3 GANs model. This model recorded a pneumonia probability of 83.04% and a normal probability of 59.28%. Although the performance is almost on par with

InceptionV3 CNN, this model shows difficulty in distinguishing between normal and pneumonia images with a higher error rate.

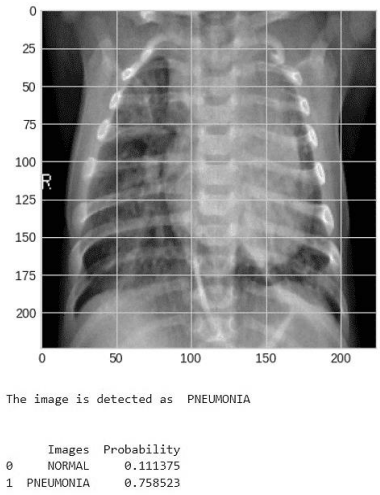

Figure 18. GANs ResNet50V2 test results

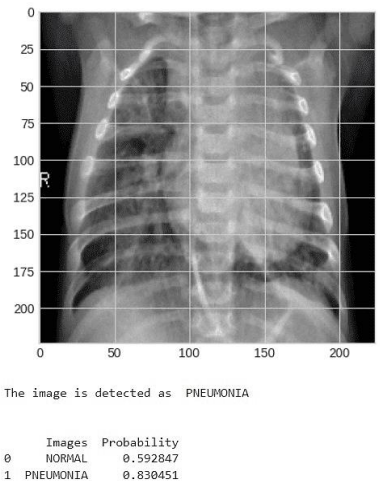

Figure 19. CNN InceptionV3 test results

The results of testing the four images above with pneumonia chest X-ray images show that each image can detect indications of pneumonia. The analysis results show that the InceptionV3 CNN model has the best percentage in detecting pneumonia with the highest probability. Although the probability value of the InceptionV3 GAN model is almost the same, this model still has difficulty distinguishing normal pneumonia images from normal images. Meanwhile, the CNN ResNet50V2 and GANs ResNet50V2 models have the same pneumonia probability value and normal probability value.

4. CONCLUSION

In this work, we assessed how well two architectures CNN and GAN performed in diagnosing pneumonia. When training the models, we employed techniques for both transfer learning and fine-tuning. Following the training phase, we compared the test outcomes of the two topologies for each algorithm. The test findings demonstrate that, with an accuracy of 94% on the CNN algorithm, the ResNet50V2 design outperforms the InceptionV3 architecture, whereas the latter only managed a 93% accuracy. Furthermore, the test results on the GANs algorithm show that the ResNet50V2 architecture is superior to the InceptionV3 architecture with an accuracy of 96%, while the InceptionV3 architecture achieved an accuracy of 92%. In the CNN algorithm, the ResNet50V2 architecture detects pneumonia cases better than the InceptionV3 architecture, and the GAN algorithm is also better. The strengths of this study include the use of deep learning techniques that proved effective, the integration of GANs that helped overcome overfitting, and the comprehensive evaluation of various model combinations. Nevertheless, there were some drawbacks to this study as well. For instance, although the ResNet50V2 model's accuracy increased when GANs were used, the accuracy decreased when GANs were used with InceptionV3. Furthermore, the accuracy of the model was the main emphasis of this study rather than a thorough examination of how the model was incorporated into current clinical workflows or how it affected radiologists' medical judgments. By doing this, we intend to better diagnose pneumonia from chest X-ray pictures by using the strengths of both designs. For future research, it is recommended to integrate more transfer learning architectures, such as DenseNet121 or Xception, which were previously shown to have high performance in medical image classification. In addition, it is necessary to explore more complex data augmentation methods to enrich the variety of training data, so that the model can be more robust in handling new data.

REFERENCES

[1] M. M. Hasan, M. M. J. Kabir, M. R. Haque, and M. Ahmed, “A combined approach using image processing and deep learning to detect pneumonia from chest X-ray image,” in 2019 3rd international conference on electrical, Computer & Telecommunication Engineering (ICECTE), IEEE, 2019, pp. 89–92.

[2] M. Aydogdu, E. Ozyilmaz, H. Aksoy, G. Gursel, and N. Ekim, “Mortality prediction in community-acquired pneumonia requiring mechanical ventilation; values of pneumonia and intensive care unit severity scores,” Tuberk Toraks, vol. 58, no. 1, pp. 25–34, 2010.

[3] B. PRUITT, “Pneumonia: Etiology, Care and Prevention.,” RT: The Journal for Respiratory Care Practitioners, vol. 37, no. 4, 2024.

[4] Q. An, W. Chen, and W. Shao, "A Deep Convolutional Neural Network for Pneumonia Detection in X-ray Images with Attention Ensemble," Diagnostics, vol. 14, no. 4, p. 390, 2024.
[5] M. I. Neuman et al., "Variability in the interpretation of chest radiographs for the diagnosis of pneumonia in children," J Hosp Med, vol. 7, no. 4, pp. 294–298, 2012.
[6] R. M. Hopstaken, T. Witbraad, J. M. A. Van Engelshoven, and G. J. Dinant, "Inter-observer variation in the interpretation of chest radiographs for pneumonia in community-acquired lower respiratory tract infections," Clin Radiol, vol. 59, no. 8, pp. 743–752, 2004.
[7] W. H. Organization, "Standardization of interpretation of chest radiographs for the diagnosis of pneumonia in children," World Health Organization, 2001.
[8] D. Hastari, S. Winanda, A. R. Pratama, N. Nurhaliza, and E. S. Ginting, "Application of Convolutional Neural Network ResNet-50 V2 on Image Classification of Rice Plant Disease," Public Research Journal of Engineering, Data Technology and Computer Science, vol. 1, no. 2, 2024.
[9] D. Srivastav, A. Bajpai, and P. Srivastava, "Improved classification for pneumonia detection using transfer learning with GAN based synthetic image augmentation," in 2021 11th international conference on cloud computing, data science & engineering (confluence), IEEE, 2021, pp. 433–437.
[10] P. D. Rinanda, D. N. Aini, T. A. Pertiwi, S. Suryani, and A. J. Prakash, "Implementation of Convolutional Neural Network (CNN) for Image Classification of Leaf Disease In Mango Plants Using Deep Learning Approach," Public Research Journal of Engineering, Data Technology and Computer Science, vol. 1, no. 2, pp. 56–61, 2024.
[11] A. Krizhevsky, I. Sutskever, and G. E. Hinton, "Imagenet classification with deep convolutional neural networks," Adv Neural Inf Process Syst, vol. 25, 2012.
[12] V. Sirish Kaushik, A. Nayyar, G. Kataria, and R. Jain, "Pneumonia detection using convolutional neural networks (CNNs)," in Proceedings of First International Conference on Computing, Communications, and Cyber-Security (IC4S 2019), Springer, 2020, pp. 471–483.
[13] A. Madhavi, M. S. Abhijna, P. Sumanjali, S. Supraja, M. Ghalwan, and M. R. Chary, "Automated Diagnosis of Pneumonia Using CNN and Transfer Learning Approaches," in E3S Web of Conferences, EDP Sciences, 2023, p. 01031.
[14] X. Liu and C.-J. Hsieh, "Rob-gan: Generator, discriminator, and adversarial attacker," in Proceedings of the IEEE/CVF conference on computer vision and pattern recognition, 2019, pp. 11234–11243.
[15] S. Vashisht, S. Lamba, B. Sharma, and A. Sharma, "Pneumonia classification using CNN-GAN," in 2023 International Conference on Sustainable Computing and Data Communication Systems (ICSCDS), IEEE, 2023, pp. 456–461.
[16] A. U. Ibrahim, M. Ozsoz, S. Serte, F. Al-Turjman, and P. S. Yakoi, "Pneumonia classification using deep learning from chest X-ray images during COVID-19," Cognit Comput, vol. 16, no. 4, pp. 1589–1601, 2024.
[17] E. Ayan and H. M. Ünver, "Diagnosis of pneumonia from chest X-ray images using deep learning," in 2019 Scientific meeting on electrical-electronics & biomedical engineering and computer science (EBBT), Ieee, 2019, pp. 1–5.
[18] P. Rajpurkar, "CheXNet: Radiologist-Level Pneumonia Detection on Chest X-Rays with Deep Learning," ArXiv abs/1711, vol. 5225, 2017.
[19] D. Kermany, "Labeled optical coherence tomography (oct) and chest x-ray images for classification," Mendeley data, 2018.
[20] K. Kallianos et al., "How far have we come? Artificial intelligence for chest radiograph interpretation," Clin Radiol, vol. 74, no. 5, pp. 338–345, 2019.
[21] N. A. Andriyanov, "Analysis of the acceleration of neural networks inference on intel processors based on openvino toolkit," in 2020 Systems of Signal Synchronization, Generating and Processing in Telecommunications (SYNCHROINFO), IEEE, 2020, pp. 1–5.
[22] C. Bailer, T. Habtegebrial, and D. Stricker, "Fast feature extraction with CNNs with pooling layers," arXiv preprint arXiv:1805.03096, 2018.
[23] L. Engstrom, B. Tran, D. Tsipras, L. Schmidt, and A. Madry, "A rotation and a translation suffice: Fooling cnns with simple transformations," 2017.
[24] S. Reed, Z. Akata, X. Yan, L. Logeswaran, B. Schiele, and H. Lee, "Generative adversarial text to image synthesis," in International conference on machine learning, PMLR, 2016, pp. 1060–1069.
[25] C. Ledig et al., "Photo-realistic single image super-resolution using a generative adversarial network," in Proceedings of the IEEE conference on computer vision and pattern recognition, 2017, pp. 4681–4690.
[26] P. Isola, J.-Y. Zhu, T. Zhou, and A. A. Efros, "Image-to-image translation with conditional adversarial networks," in Proceedings of the IEEE conference on computer vision and pattern recognition, 2017, pp. 1125–1134.
[27] H. Wu, S. Zheng, J. Zhang, and K. Huang, "Gp-gan: Towards realistic high-resolution image blending," in Proceedings of the 27th ACM international conference on multimedia, 2019, pp. 2487–2495.

[28] R. A. Yeh, C. Chen, T. Yian Lim, A. G. Schwing, M. Hasegawa-Johnson, and M. N. Do, "Semantic image inpainting with deep generative models," in Proceedings of the IEEE conference on computer vision and pattern recognition, 2017, pp. 5485–5493.
[29] I. Goodfellow et al., "Generative adversarial nets," Adv Neural Inf Process Syst, vol. 27, 2014.
[30] A. K. Jaiswal, P. Tiwari, S. Kumar, D. Gupta, A. Khanna, and J. J. P. C. Rodrigues, "Identifying pneumonia in chest X-rays: A deep learning approach," Measurement, vol. 145, pp. 511–518, 2019.
[31] K. He, X. Zhang, S. Ren, and J. Sun, "Identity mappings in deep residual networks," in Computer Vision–ECCV 2016: 14th European Conference, Amsterdam, The Netherlands, October 11–14, 2016, Proceedings, Part IV 14, Springer, 2016, pp. 630–645.
[32] S. S. S. Koushik and K. G. Srinivasa, "Detection of respiratory diseases from chest X rays using Nesterov accelerated adaptive moment estimation," Measurement, vol. 176, p. 109153, 2021.